Chapter 1

Single shot emittance measurement

1.1 Motivation

The publications about the dream beams in 2004 [1, 2, 3], the Oxford-Berkeley results in 2006 [4] and energy doubling experiment at SLAC in 2007 [5] triggered a strong interest for the beams produced by plasma acceleration, both laser-driven and beam-driven.

Starting in 2006 I decided to look at the development of advanced diagnostics to measure some of the parameters of these beams. One of the key difference between conventional beam and those produced by plasma accelerator is the reproducibility: beam produced by plasma accelerators are not as stable as those produced in conventional accelerators.

My focus has been the measurements of the Emittance Transverse and Longitudinal of these beams. This work is described in this chapter and the next respectively. In the second-next chapter I will mention laser-plasma experiments in which I took part.

1.2 Transverse emittance of a laser-driven plasma accelerator

In [4] the transverse size of the beam at the source is limited by the laser size ($r_s < 35\,\mu m$). Its divergence has been measured as less than 2 mrad (r.m.s.). This gives a geometric emittance of 70 µm mrad at 1.0 GeV and a normalized emittance of 35 nm mrad. Such transverse emittance , if confirmed, would be rather compared to what is usually produced on conventional linacs.

However the measurement of such emittance is very difficult because, as noted by the authors of [4] the beam has a high energy and is rather unstable and therefore each shot is different.

The emittance of a beam is a measure of its quality (or of the relative movement of the electrons in the beam with respect to each other). It is the product of the beam size by its divergence at a waist and it can therefore be compared to the temperature of a gas (which is also the product of the size [volume] by the divergence [thermal agitation or pressure]).

In conventional accelerators the emittance can be measured in different ways. At low energy single shot emittance measurements can be done using the "pepper-pot" method (or numerous derivatives of it). In the pepper-pot method the beam is sampled by a plate with holes (or slits) located before an imaging screen (usually a fluorescent screen) as shown on figure 1.1. As the size of each hole is well known, the spot size measured on the screen give the divergence of each beam let coming out of the holes. By looking at these local divergences any correlation induced by not being at the waist can be removed and the transverse emittance can be measured (detailed formulas are given for example in [6]).

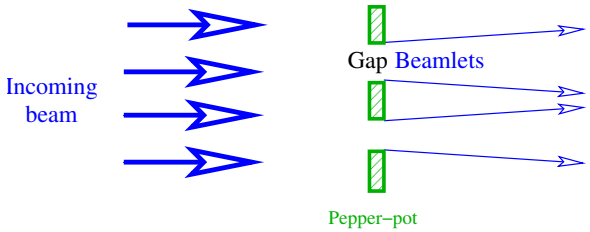

Figure 1.1: Example of a pepper-pot sampling a beam into several beamlets. The transverse emittance is given by using the hole size and the beamlets divergence measured on the screen (image taken from [7]).

At high energy the beam would easily go through the sampling plate used and therefore other methods are favored. Quadrupole scans allow to measure the transverse emittance by looking at beam size variation on a screen with the intensity of a focusing quadrupole is changed. However this requires several shots to be performed consecutively and this is not possible with an accelerator where the beam energy and pointing change from shot to shot.

A variation of the quadrupole scan method is the multiscreen method where the beam size is measured by screens (or laser-wires) in several locations along the beam trajectory. By looking at how the beam size evolves as it propagates and by using the known beam optics it is possible to calculate the beam transverse emittance. As each screen may significantly scatter the beam this method is usually only used in accelerators where the beam is stable.

As none of the conventional emittance measurement methods were available for laser-

plasma accelerators I decided to see how they could be adapted to perform such measurement. The goal being to measure the transverse emittance of high energy (several hundreds MeV) beam in a single shot. This led me to two different developments: extended pepper-pots, described in section 1.3 and Multiple OTR described in section 1.4.

1.3 Extended pepper-pot

A solution to use pepper-pot at high energies would be to increase the thickness of the plate. I decided to investigate this both theoretically and experimentally.

As I did not have any experience with Pepper-pot measurements the first step was to perform some conventional pepper-pot measurements. For that purpose I used a particle accelerator available at Oxford: the 1 MeV proton Van De Graaff teaching accelerator and together with undergraduate student Michael McCann we measured the energy of the beam [8]. The pepper-pot pattern we observed is shown on figure 1.2. At the same time, I did some simulations using the GEANT4 software [9] with undergraduate student Joe Hewlett to make sure that such thick pepper-pot would still allow to measure the beam emittance [10].

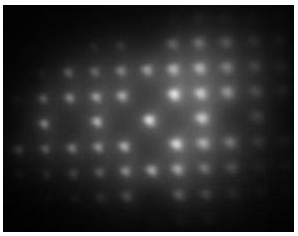

Figure 1.2: Example of pepper-pot measurement using the Oxford teaching accelerator (image taken from [8]).

Building on this initial work we decided to prepare an experimental campaign to test thick pepper-pots at high energy. For these tests we obtained beam time at the Beam Test Facility (BTF) [11, 12, 13] of the Frascati National Laboratory (INFN/LNF).

Our experiment is described in details in [14]. Here is a brief summary of the experiment as taken from that reference: For our experiment the beam line was extended by more than two metres after the final bending magnet. The pepper-pot was fitted on an actuator mounted inside a 4-way cross installed 2.2 m after the bending magnet. The pepper-pot could be inserted when emittance measurement were being made or retracted to allow for other studies to take place. A YAG screen located 230 mm after the pepper-pots was used to ensure proper alignment. The test facility vacuum ended 380 mm after the pepper-pot with a 50 µm mylar window. The electrons were detected by a gadolinium doped screen (?Lanex regular?) produced by Kodak located 200 mm beyond the mylar window. The photons emitted by the lanex screen were reflected by a 45° mirror and

recorded by a camera located 672 mm away from the screen. The lens fitted on this camera was focussed on the lanex screen. This arrangement allowed the camera to be out of the accelerator plane and shielded from the radiation by lead bricks. The layout of the experiment is shown on figure 1.3.

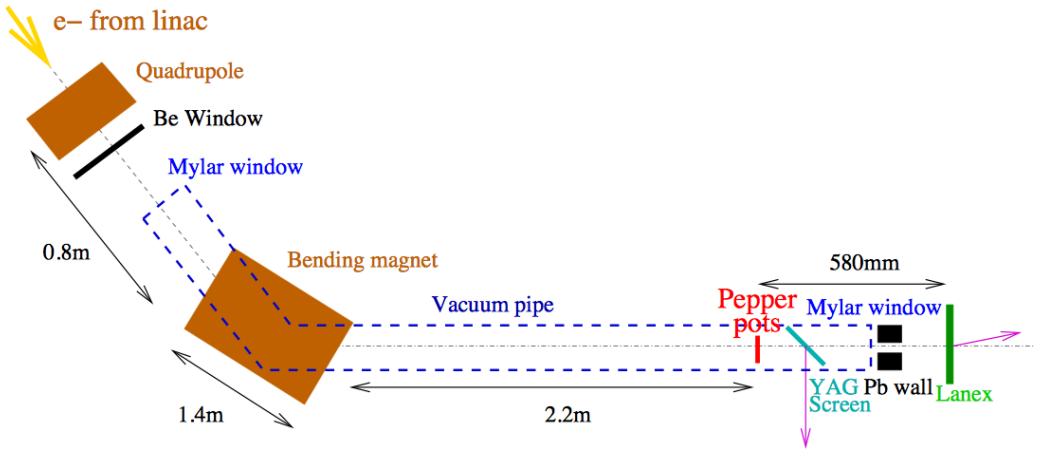

Figure 1.3: Layout of the pepper-pot experiment at the BTF as shown in [14].

A picture of the pepper-pot used is shown on figure 1.4 and example of the data measured during that experiment are shown in figure 1.5.

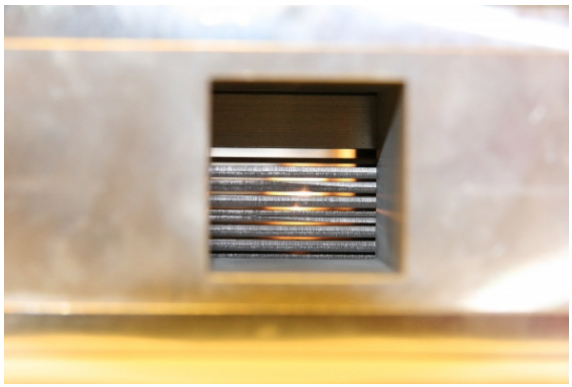

Figure 1.4: Picture of the pepper-pot used at the BTF as shown in [14].

The success of this experiment led us to plan a similar experiment in the transfer line from the booster to the synchrotron of the DIAMOND Light Source. At that location the beam could reach an energy of up to 3 GeV and we performed experiments at 2 GeV and 3 GeV. The observed pattern and the stability of the measurement are shown on figure 1.6. These results have been published in [15].

I also investigated how to apply this technique to protons with measurements on LINAC2 at CERN.

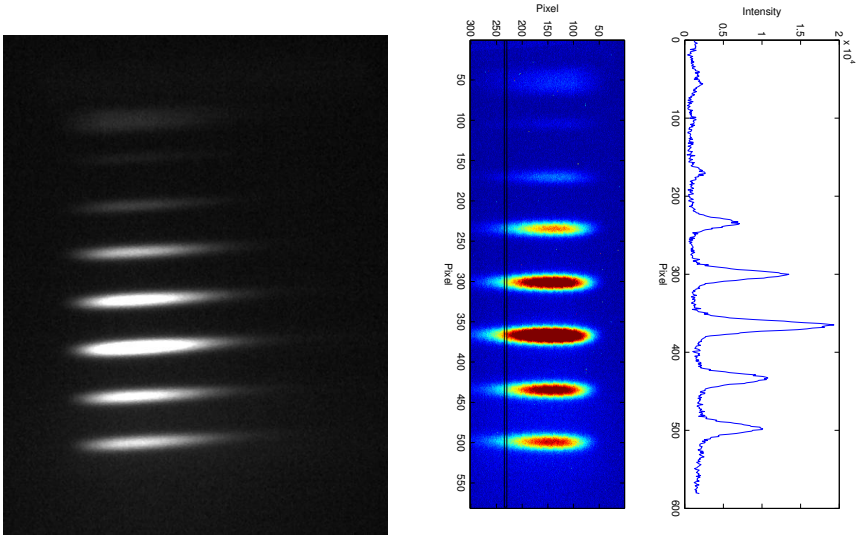

Figure 1.5: Example of pepper-pots measurements similar to those reported in [14]. Left: image measured by the camera. Right False colors image and slits profiles.

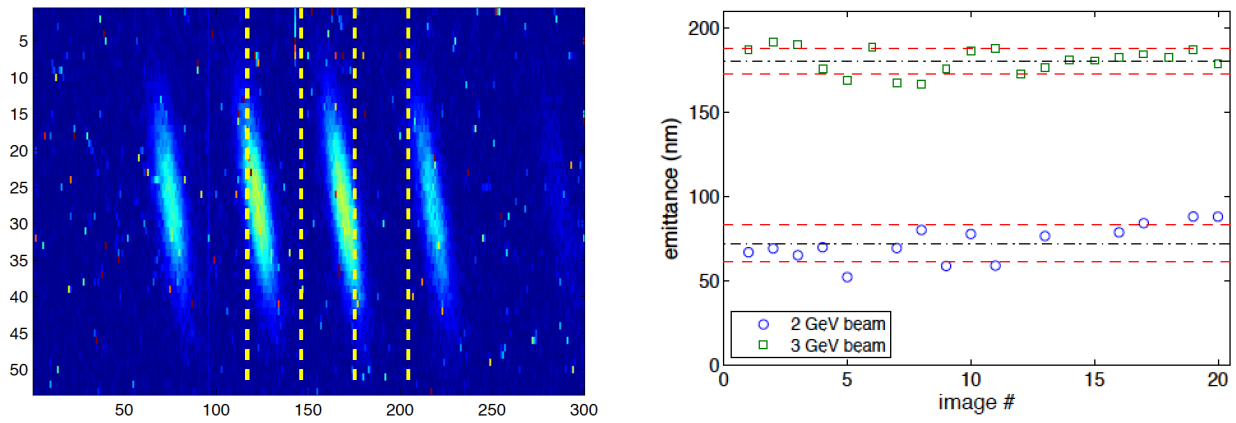

Figure 1.6: XXX Example of pepper-pots measurements similar to those reported in [14]. Left: image measured by the camera. Right False colors image and slits profiles.

- Image CERN XXXXXXXXXXXXXXX

One of the concerns with that technique expressed several times during conferences was that the length of the pepper-pot channel might biais the emittance measurement. To validate my approach I made several calculations and GEANT4 simulations. The calculations have been published in [7] and I reproduced below the main arguments taken from [7] and encourage the interested reader to refer to the full publication.

The main problem of using a Pepper-pot as diagnostic for transverse emittance measurement of high energy particles, arises from the thickness of material required to give sufficient contrast between the beam passing through the hole and the stopped beam. The thickness of material needed to stop electrons with an energy of several hundreds of MeV is quite large. Although one radiation length is enough to absorb in average all but $1/e$ of the electrons' energy [16], the GEANT4 [9] simulations shown in figure 1.7 indicate that several additional radiation lengths are required to stop most of the electronic shower. Therefore, a pepper-pot able to measure the transverse emittance of a beam of several hundred MeV electrons must have a significant longitudinal extent (figure **??**) and one may question how the acceptance of the pepper-pot is modified by this length.

The figure 1.8 shows how the phase-space evolves as a bunch of particles propagates through a long pepper-pot and figure 1.9 shows GEANT4 simulations validating the work. The conclusions of these calculations were that provided that the parameters are chosen correctly (and the constraints on such choice are not too stringer) it is valid to use an extended pepper-pot to measure the transverse emittance of a high energy beam.

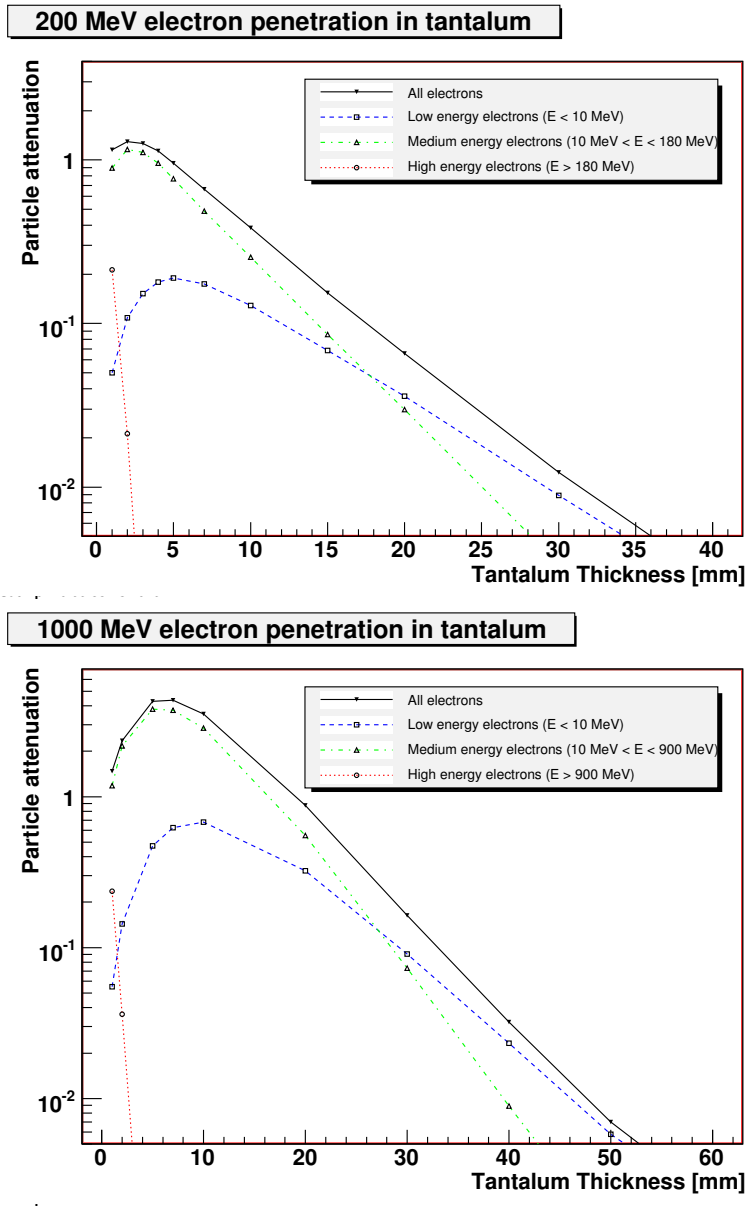

Figure 1.7: GEANT4 [9] simulations of the penetration of high energy electrons in a block of Tantalum. The horizontal axis gives the penetration depth and the vertical axis gives the number of electrons remaining at that depth for one initial electron. The red lines (round markers) correspond to high energy electrons whereas the blue lines (square markers) and the green lines (up-pointing triangular markers) correspond to lower energy particles emitted by the initial particle. The black lines (down-pointing triangular markers) show the total number of electrons remaining. The plot on the top corresponds to 200 MeV electrons and the one on the bottom to 1 GeV electrons. Figure taken from [7].

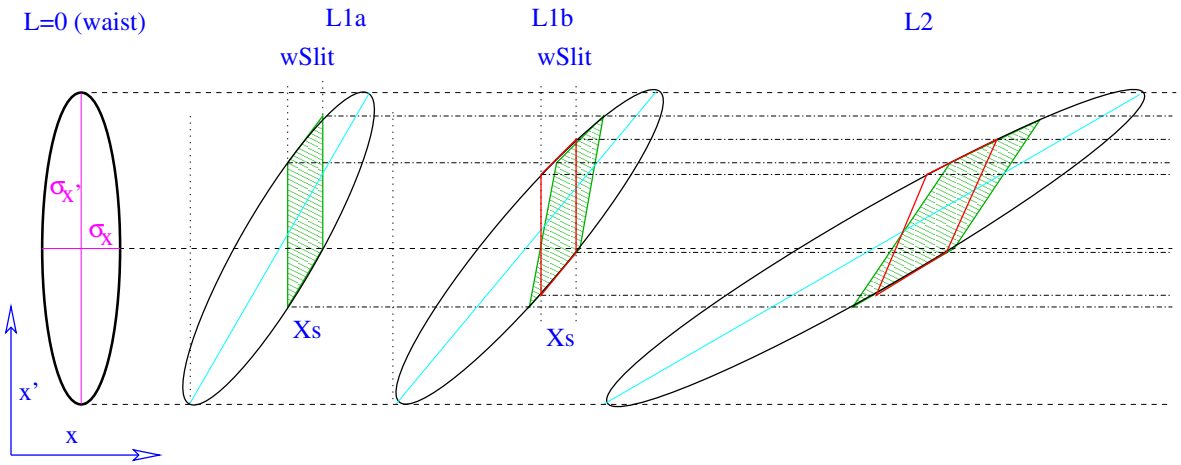

Figure 1.8: Long pepper-pot: Evolution of the phase-space as the beam drifts. At the source or at a wait ($L = 0$) the phase space of the beam is first represented by an upright ellipse. As the beam drifts the ellipse gets sheared. At L_{1a} the beam enters a slit and thus only the particles in the green area pass the slit. While the beam travels in the slit the ellipse is further sheared, hence at L_{1b}, the exit of the slit, the area of phase space within the slit acceptance (red box) is different from that occupied by the particles sampled at the entrance of the slit. Hence the full acceptance of the slit correspond to the overlap between the green and the red areas. Figure taken from [7]. The variables definition is given in [7].

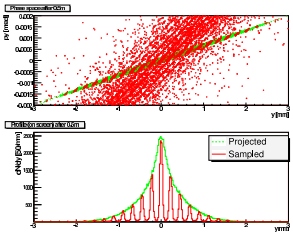

$\Delta L_{ba} = 10\,\text{mm};\ \frac{\mathcal{A}_s - \mathcal{A}_o}{\mathcal{A}_o} = 4.5\%$

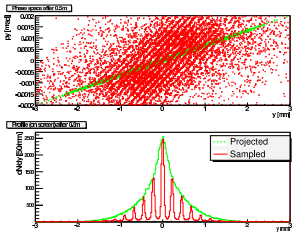

$\Delta L_{ba} = 50\,\text{mm};\ \frac{\mathcal{A}_s - \mathcal{A}_o}{\mathcal{A}_o} = 22.5\%$

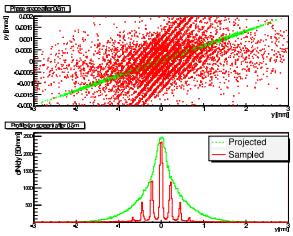

$\Delta L_{ba} = 100\,\text{mm};\ \frac{\mathcal{A}_s - \mathcal{A}_o}{\mathcal{A}_o} = 45\%$

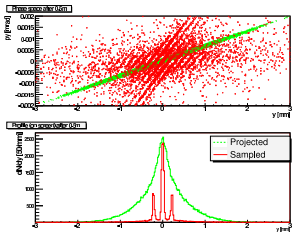

$\Delta L_{ba} = 200\,\text{mm};\ \frac{\mathcal{A}_s - \mathcal{A}_o}{\mathcal{A}_o} = 90\%$

$w_{\text{slit}} = 50\,\mu\text{m};\ \sigma_x = 50\,\mu\text{m}\ ;\sigma_{x'} = 0.5\,\text{mrad};$
$L_{1a} = 1\,\text{m};\ L_2 = 1.5\,\text{m};\ 1\,\text{GeV};\ 100\ 000\ \text{electrons}$

Figure 1.9: Reconstruction of the transverse phase space of a beam sampled by a long pepper-pot. In each pair of plots the top plot shows in green the original phase space of the electrons and in red the phase space of the electrons after the pepper-pot. In each pair the bottom plot shows the projection along the spatial component of the transverse phase space. In all these plots the beam energy is 1 GeV. The slit width is 50 µm, the beam size at the waist is 100 µm with a divergence of 1 mrad and the pepper-pot are located 1 m away from the beam waist. The screen is located 500 mm after the pepper-pot. For each plot 100 000 electrons were simulated with GEANT4. The top left pair of plots corresponds to a pepper-pot length of 10 mm, the top right pair of plots corresponds to a pepper-pot length of 50 mm, the bottom left pair of plots corresponds to a pepper-pot length of 100 mm and the bottom right pair of plots correspond to a pepper-pot length of 200 mm. For each plot the value of $\frac{\mathcal{A}_s - \mathcal{A}_o}{\mathcal{A}_o}$ as defined in equation **??** is given. High energy photons (X-rays) are not shown on this figure. Figure taken from [7].

1.4 Multiple OTR measurement to measure the transverse emittance of a beam

As the energy of the beam gets higher the thickness of material required to stop the beam will be larger so a different technique had to be found. I decided to look for a solution to perform multiple screen emittance measurement with each screen setup so that its disturbance of the beam is negligible. This is possible using Optical Transition Radiation (OTR)[17, 18] : as it is a surface effect, it does not depend on the thickness of the material used. The first condition to validate this idea of single shot transverse emittance measurement using multiple OTR screens was to check what would be the impact of several screen on the emittance and, reciprocally what would be the maximum acceptable thickness for such measurement.

I reproduce below the text of an unpublished note written to make the estimates, some of which was latter included in a publication [19]. This note was written with the help of Cyrille Thomas and Riccardo Bartolini who were both at the Diamond Light Source at that time.

For our calculations we use the layout shown on figure 1.10: 3 screens located 0.5 m apart from each other followed by a 4th screen located 1 m beyond the 3rd screen.

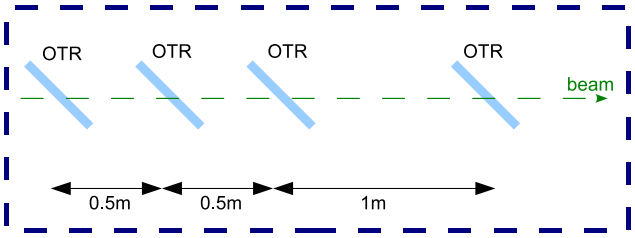

Figure 1.10: Screen layout used in the calculations of multiple OTR single shot emittance measurement.

1.4.1 Beam propagation in a drift space

In a drift space the beam (σ) size evolves as [20]:

$$\sigma(s) = \sqrt{\epsilon(\beta_0 - 2\alpha_0 s + \gamma_0 s^2)} \tag{1.1}$$

where s is the position in the drift space, α_0, β_0 and γ_0 are the Twiss parameters at $s = 0$ and ϵ is the beam emittance.

When $s = 0$ is a symmetry point (waist), this can be rewritten as

$$\sigma(s) = \sqrt{\epsilon\beta_0 + \frac{\epsilon}{\beta_0}s^2} \tag{1.2}$$

hence

$$\sigma^2(s) = \epsilon\beta_0 + \frac{\epsilon}{\beta_0}s^2 \tag{1.3}$$

By measuring σ with an OTR screen at 3 (or more) locations around a waist it is thus possible to make a parabolic fit giving the Twiss parameters of the beam as well as ϵ and β_0. Equation 1.3 shows that a linear fit of s^2 versus the beam sizes squared will also give the beam emittance.

1.4.2 Beam expansion condition

In such drift space the beam divergence is (with a different sign on either side of the waist)

$$\sigma' = \pm\sqrt{\frac{\epsilon}{\beta}} = \pm\frac{\epsilon}{\sigma_0} \tag{1.4}$$

with σ_0 the beam size at the waist.

The beam size at a given distance s from the waist will be related to the beam size at the waist by the following relation:

$$\begin{aligned} \frac{\sigma(s)}{\sigma_0} &= \frac{\sqrt{\epsilon\beta_0 + \frac{\epsilon}{\beta_0}s^2}}{\sqrt{\epsilon\beta_0}} \\ &= \sqrt{1 + \frac{s^2}{\beta_0^2}} \end{aligned} \tag{1.5}$$

Using $\beta_0 = \frac{\sigma_0^2}{\epsilon}$, this becomes:

$$\frac{\sigma(s)}{\sigma_0} = \sqrt{1 + \frac{\epsilon^2 s^2}{\sigma_0^4}} \tag{1.6}$$

Hence for a 1 mm.mrad beam with a 1 mm spot size, the beam will have increased by 10% beam at $s = 0.45$ m and by 20% at $s = 0.66$m. For the same beam with a 5mm spot size, these distances are multiplied by 25 and become $s = 11.46$m and $s = 16.6$m.

1.4.3 Effect of the scattering in the screens on the beam expansion

An electron traversing nuclear matter will be Coulomb scattered. Most of these scattering will be at very small angle but will add up as the electron progresses through the matter. The phenomena is described in details in [16].

For a bunch of electron, the scattering experienced after traversing a layer of thickness x can be approximated by a Gaussian of width[21]:

$$\theta_0 = \frac{13.6 \text{ MeV}}{\beta cp}\sqrt{\frac{x}{X_0}}\left[1 + 0.038ln\left(\frac{x}{X_0}\right)\right] \tag{1.7}$$

where βc is the velocity of the electrons, p their momentum and X_0 a quantity called the radiation length and which expresses how high energy electrons loose their energy in a given material[1].

To make it easier to estimate the scattering as a function of the momentum this equation can be rewritten as

$$p\theta_0 = \frac{13.6 \text{ MeV}}{\beta c}\sqrt{\frac{x}{X_0}}\left[1 + 0.038ln\left(\frac{x}{X_0}\right)\right] \tag{1.8}$$

Table 1.1 shows that the electrons will travel only a small fraction of a radiation length (X_0) in each type of screen considered. A scattering factor $p\theta_0$ of the order of a hundred MeV.mrad means that a beam with an energy of a hundreds MeV will be scattered by about one milliradian. Among the different screens considered, Mylar and Kapton (Polyimide film) introduce the lower scattering and thinner films seems available.

When the beam scatters on the screens an additional scattering term is required and equation 1.1 is approximately modified as follow:

$$\sigma(s) = \sqrt{\epsilon(\beta_0 - 2\alpha_0 s + \gamma_0 s^2)} + \sum_{i=1}^{N(s)\text{screens}} (s - s_i)\theta_i^2 \tag{1.9}$$

where $N(s)_{\text{screens}}$ is the number of screens located upstream from the position at which the measurement is performed, s_i their position and θ_i the scattering they induce.

Assuming that all screens are made of the same material with a scattering coefficient θ_0, the scattering induced by the first screen will dominate:

[1] The radiation length is the mean distance over which a high-energy electron looses all but $1/e$ of its energy by Bremstrahlung[16].

Material	Radiation Length (X_0)	Thickness 10^{-4} X_0	Scattering $p\theta_0$	Limit σ_0 (eq. 1.13) $\frac{1\text{mm.mrad}}{\theta_0}$
Aluminium (10 μm)	8.9 cm	1.12	139 MeV.mrad	0.9 mm
Aluminium (30 μm)	8.9 cm	3.37	242 MeV.mrad	0.5 mm
Mylar (2 μm)	28.6 cm	0.069	34 MeV.mrad	3.7 mm
Mylar (5 μm)	28.6 cm	0.17	55 MeV.mrad	3.7 mm
Polyimide film (7.5 μm)	28.6 cm	0.26	66 MeV.mrad	1.9 mm
Polyimide film (10 μm)	28.6 cm	0.34	77 MeV.mrad	1.6 mm
Mylar (10 μm)	28.6 cm	0.34	77 MeV.mrad	1.6 mm
Air (2 m), 1 atm.	3 10^4 cm	66.67	1089 MeV.mrad	-
Air (2 m), 0.01 atm.	3 10^6 cm	0.67	107 MeV.mrad	-

Table 1.1: Nuclear properties of various materials [16] for different thicknesses. The last column is for a 500 MeV beam with a transverse emittance of 1.mm.mrad.

$$\sum_{i=1}^{N(s)\text{screens}} (s - s_i)\theta_i \simeq (s - s_1)\theta_0 \tag{1.10}$$

A measurement of the beam size dominated by the term $(s - s_1)\theta_0$ will provide information on the scattering but not on the emittance of the beam. Hence the screens, their position and the beam optics must be chosen so that in all measurements the scattering can be neglected.

This requires:

$$\frac{\epsilon}{\sigma_0} s > N_{\text{screens}} \theta_0 (s - s_1) \tag{1.11}$$

where N_{screens} is the total number of screens used.

Assuming that the first screen is close from the waist and hence $s - s_1 \simeq s$, this can be rewritten as:

$$\frac{\epsilon}{\sigma_0} >> N_{\text{screens}} \theta_0 \tag{1.12}$$

$$\sigma_0 << \frac{\epsilon}{N_{\text{screens}} \theta_0} \tag{1.13}$$

Equation 1.13 can be rewritten as

$$\sigma_0 << N_{\text{screens}} \frac{\epsilon_n}{\gamma \frac{p\theta_0}{p}} \tag{1.14}$$

$$\sigma_0 << N_{\text{screens}} \frac{mc\epsilon_n}{p\theta_0} \tag{1.15}$$

where ϵ_n is the normalised emittance, γ the Lorentz transformation factor and c the speed of light.

This shows that the requirement on σ_0 as a function of the normalised emittance and of $p\theta_i$ is independent of the beam energy (but the ease of achieving a given σ_0 may be different).

At 500 MeV a 7.5μm polyimide film screen will induce a scattering $\theta_i = 0.13$mrad. With an emittance $\epsilon = 1$mm.mrad, equation 1.13 requires $\sigma_0 << 7.6$mm. The limit value of σ_0 as given by equation 1.13 assuming $N_{\text{screens}} = 4$ for various screen materials is given in table 1.1.

When the spot size is chosen so that equation 1.13 is satisfied the scattering can be neglected, it is the case with thin Mylar or kapton screens .

1.4.4 Simulations

Mathematica

Simple simulations of such measurement have been done using Mathematica. In these simulations 4 screens were positioned at $s = -0.5m$, $s = 0m$, $s = 0.5m$ and $s = 1.5m$. The propagation of a beam with a given emittance and beta function was then calculated and the size of the beam at each screen was estimated with some noise added. To take into account the limited pixel size the measured beam size was rounded to the size of the pixels.

If the beam optics or the beam energy is not well understood the beam waist may not be positioned exactly where it is expected to be, this was included in our simulations.

Equation 1.2 was fitted to the beam sizes found and from this fit the value of the emittance was deducted. With the beam sizes used it is assumed that the effect of the scattering can be neglected as the natural beam divergence is much bigger than the divergence induced (equation 1.13).

Figure 1.11 shows a few example of such fits.

Figure 1.12 shows the difference between the deducted emittance and the real emittance for several simulation runs.

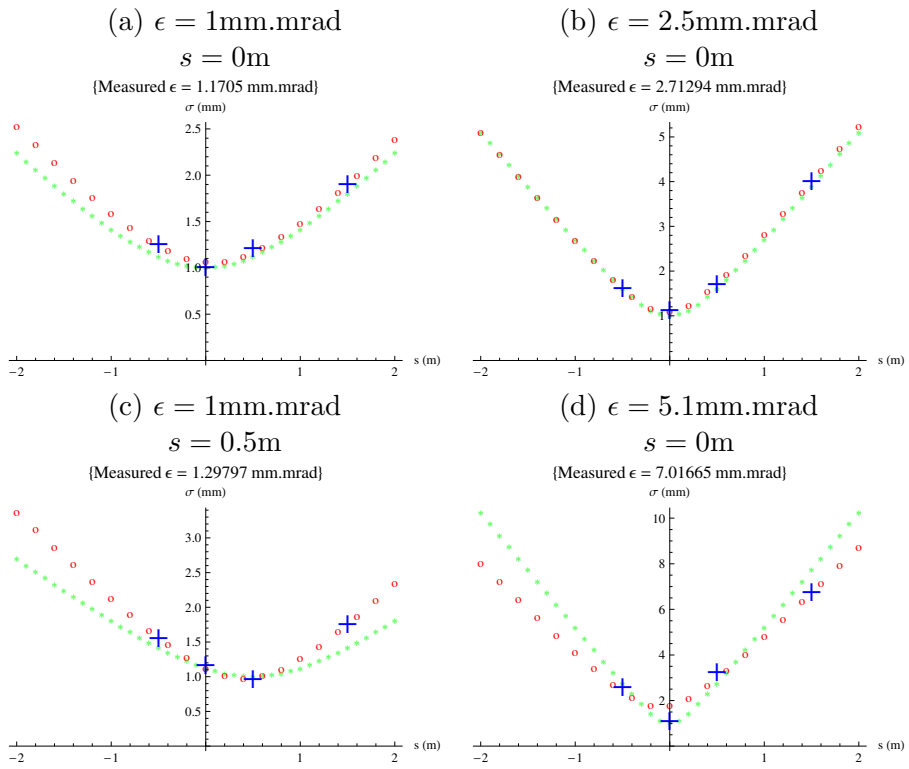

Figure 1.11: Simulated (small green dots), measured (blue crosses) and fitted (red circles) beam sizes (σ) around the waist. The beam transverse emittance (ϵ) and waist offset (s) is indicated above each plot. The waist size is always assumed to be 1 mm and the pixel size $20\mu m$. The screens used are assumed to satisfy equation 1.13 and thus the effect of the scattering is neglected in these plots.

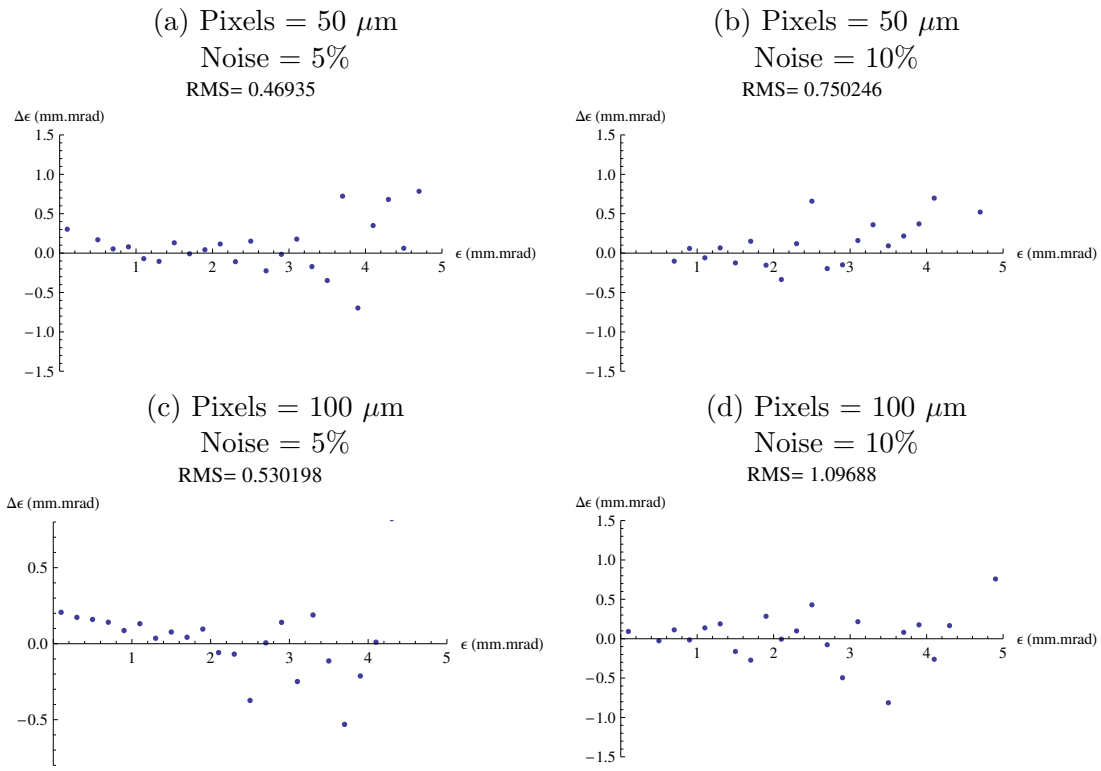

Figure 1.12: Error on the emittance measurement as a function of the beam emittance for beams forming a 1 mm waist at $s = 0$. In plots (a) and (b) the pixel size is 50 μm and in plots (c) and (d) it is 100 μm. For plot (a) and (c) the error on the beam size measurement is 5%, for plot (b) and (d) it is 10%. The screens used are assumed to satisfy equation 1.13 and thus the effect of the scattering is neglected in these plots.

Figure 1.13 shows the difference between the deducted emittance and the real emittance for several simulation runs where the waist position has been varied. These simulations show when the actual waist is far from $s = 0$ the performances of the fit are significantly degraded (this is also visible on figure **??**c).

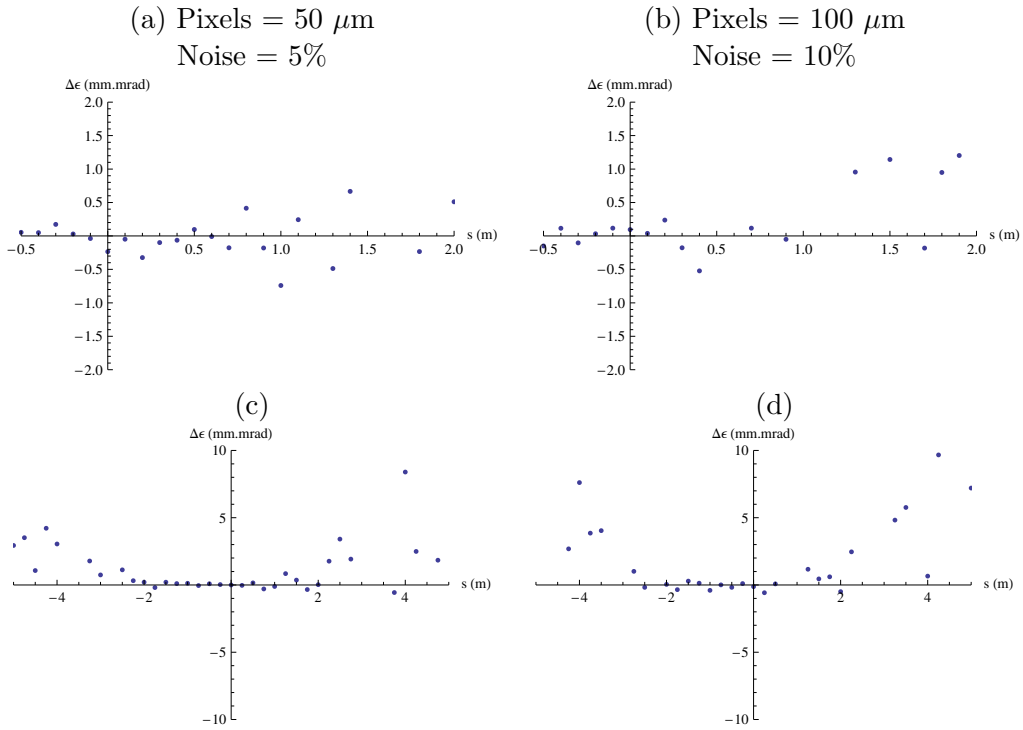

Figure 1.13: Error on the emittance measurement as a function of the position of the beam waist for beams with an emittance of 1 mm.mrad forming a 1 mm waist at the indicated position. In plot (a) and (c) the pixel size is 50 μm and the noise is 5%. In plot (b) and (d) the pixel size is 100 μm and the noise is 10%. Plot (c) and (d) repeat plat (a) and (b) over a longer range. The screens used are assumed to satisfy equation 1.13 and thus the effect of the scattering is neglected in these plots.

Geant4

To better simulate the effect of the scattering in the screens we have used the Geant4 Toolkit [9].

We have used the Geant Low Energy Physics processes [22]. These processes are valid from 250eV to 100GeV [23] and so completely cover the range of energies we are interested in.

This work was in particular done thanks to the contribution of undergraduate student Joe Hewlett. In our simulations the electrons were fired from a source on screens placed

0.5 m, 1.0 m, 1.5 m and 2.5 m after the source. The initial direction of the electrons was so that they formed a 2 mm waist 1 m after the source. A 10 µm-thick Mylar window was located 1 mm after the electron source.

The position at which the electrons traversed each screen as well as intermediate detectors was recorded. For each simulation more approximately 10 000 electrons were fired.

Emittance measurement To study the effect of the scattering in the screens several simulations were done using different materials and thicknesses for the screens. Some of the simulations for beams of 200 MeV are shown in figure 1.14 and for 500 MeV beam in figure 1.15. As one can see on the figures the use of thin Mylar screens leads to better results than with Aluminium. Furthermore thin Mylar films are easier to handle.

The previous studies assumed that the beam waist was located on the second screen. Figure 1.16 shows that the emittance can still be reconstructed with a reasonable accuracy when the waist is elsewhere (between the screens).

Commercially we found some $2\mu m$-thick Mylar coated with a 10nm layer of Aluminium. Neglecting the scattering in the aluminium, the emittance fit can be seen on figure 1.17.

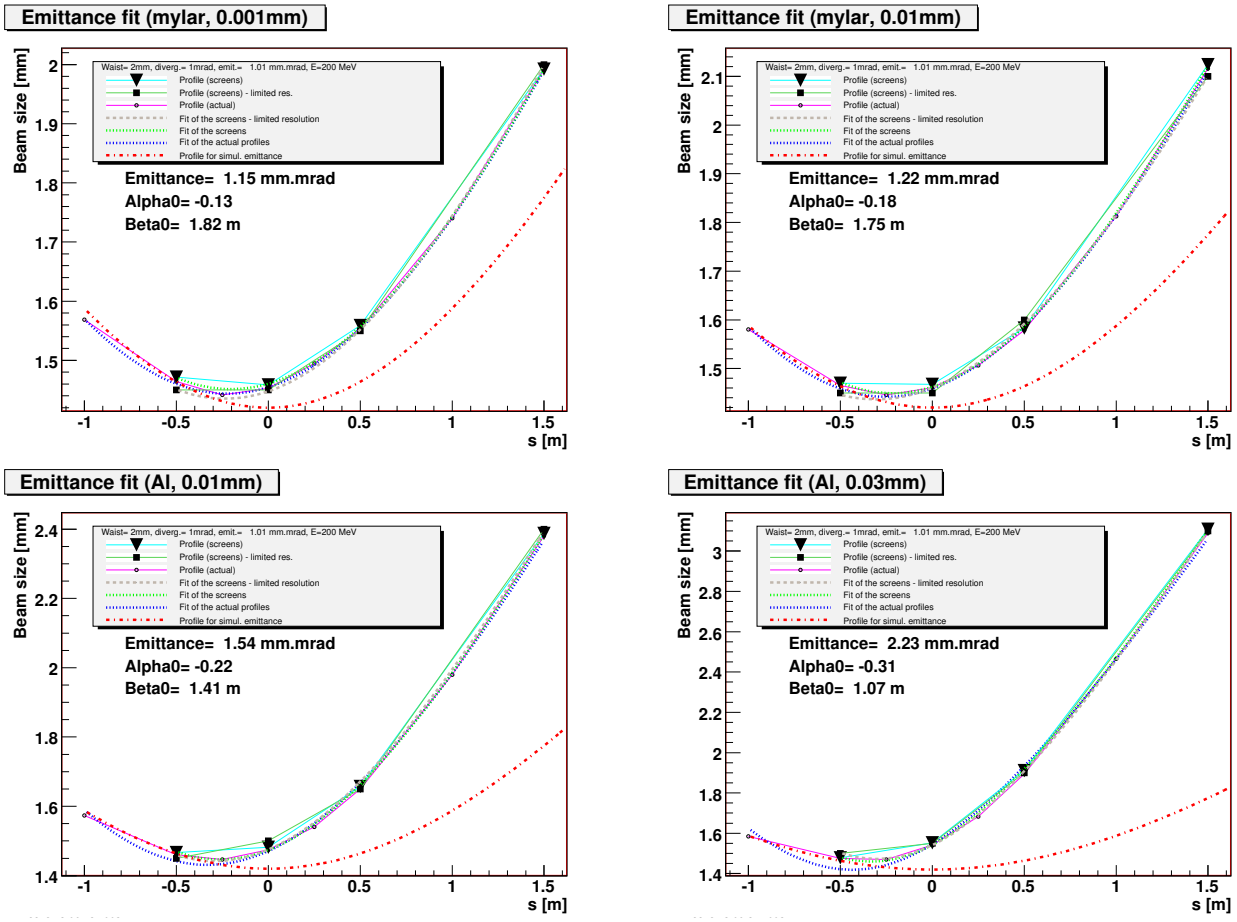

Figure 1.14: Scattering induced in a 200 MeV for various screen material and thickness with an initial emittance of 1mm.mrad. The screens material and thickness is given in the plot title. The black squares show the beam size observed on each screen, the black triangles show the beam size rounded to the nearest 50 μm (to simulate what is observed by a camera with a limited pixel size). The open circles are the position measured at additional intermediate positions. The dashed brown line shows the emittance fit made using the black triangles. The dashed green line shows the emittance fit made using the black square. The dashed green line shows the emittance fit made using the open circles. The dashed red line is the theoretical profile of the beam assuming $\alpha_0 = 0$, $\beta_0 = 2.0m$ and $\epsilon = 1.01mm.mrad$. The values given on the plot below the legend for the emittance, α_0 and β_0 are those extracted from the fit on the beam sizes with limited pixel size.

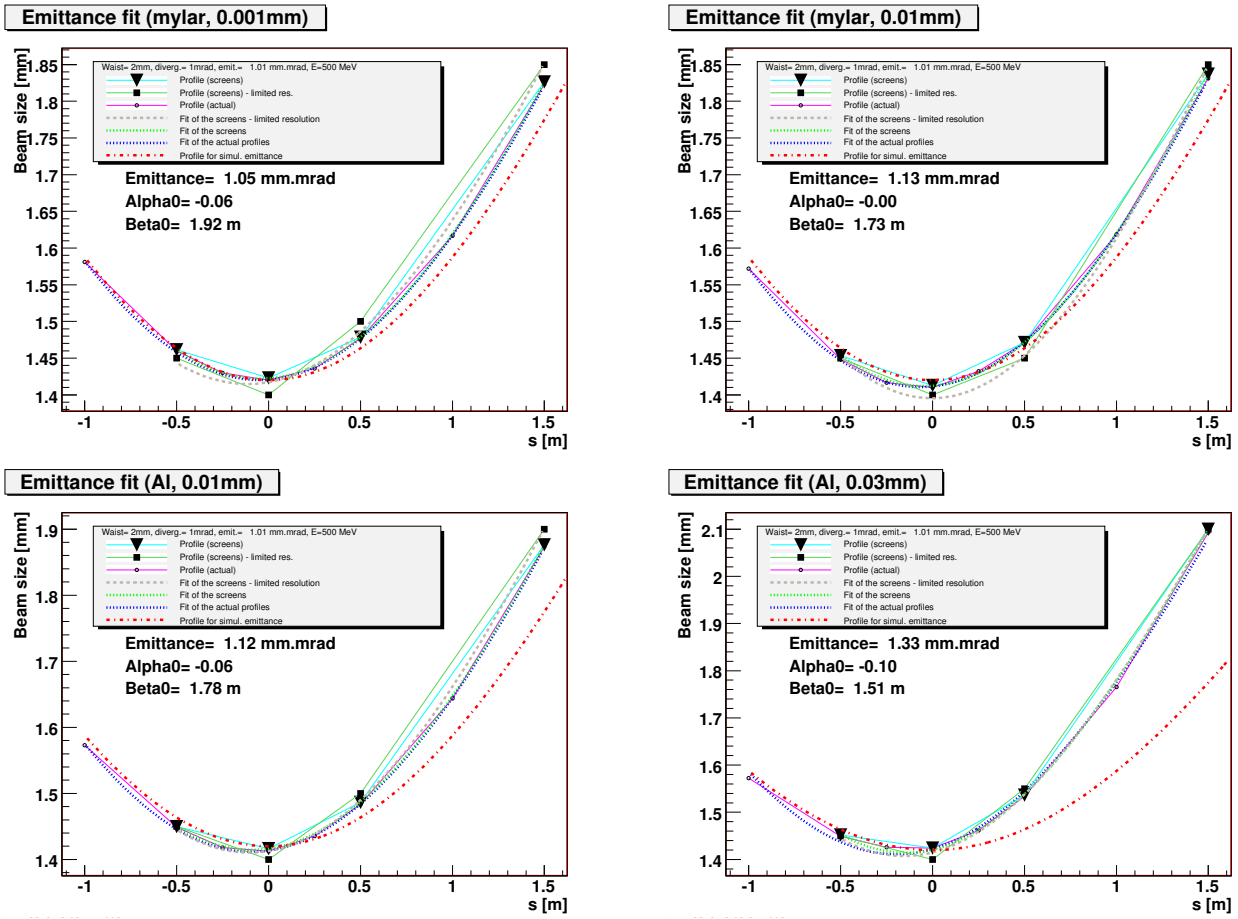

Figure 1.15: Scattering induced in a 500 MeV for various screen material and thickness with an initial emittance of 1mm.mrad. The screens material and thickness is given in the plot title. The black squares show the beam size observed on each screen, the black triangles show the beam size rounded to the nearest 50 μm (to simulate what is observed by a camera with a limited pixel size). The open circles are the position measured at additional intermediate positions. The dashed brown line shows the emittance fit made using the black triangles. The dashed green line shows the emittance fit made using the black square. The dashed green line shows the emittance fit made using the open circles. The dashed red line is the theoretical profile of the beam assuming $\alpha_0 = 0$, $\beta_0 = 2.0m$ and $\epsilon = 1.01mm.mrad$. The values given on the plot below the legend for the emittance, α_0 and β_0 are those extracted from the fit on the beam sizes with limited pixel size.

(a) -0.5m (b) +0.5m (c) +1m

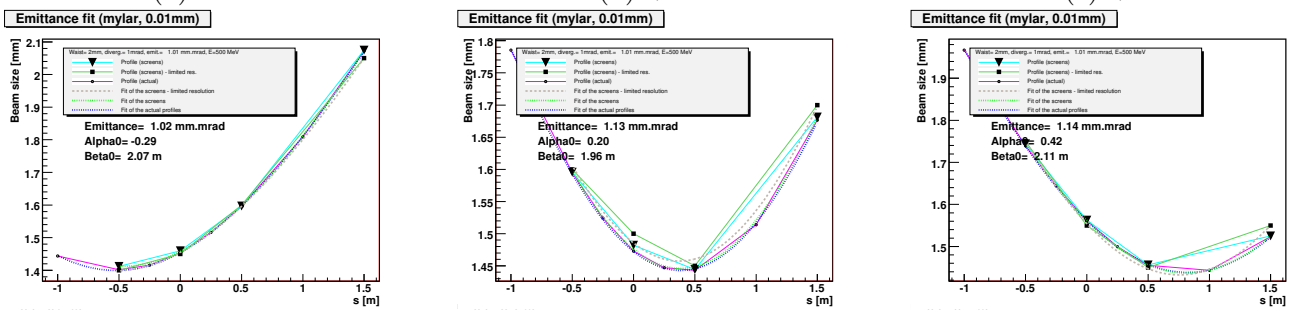

Figure 1.16: Scattering induced in a 500 MeV for $10\mu m$-thick Mylar screens for a 500 MeV beam with an initial emittance of 1mm.mrad when the waist is not located on the second screen. The waist position is given above the plot. The black squares show the beam size observed on each screen, the black triangles show the beam size rounded to the nearest 50 μm (to simulate what is observed by a camera with a limited pixel size). The open circles are the position measured at additional intermediate positions. The dashed brown line shows the emittance fit made using the black triangles. The dashed green line shows the emittance fit made using the black square. The dashed green line shows the emittance fit made using the open circles. The values given on the plot below the legend for the emittance, α_0 and β_0 are those extracted from the fit on the beam sizes with limited pixel size.

(a) 200 MeV

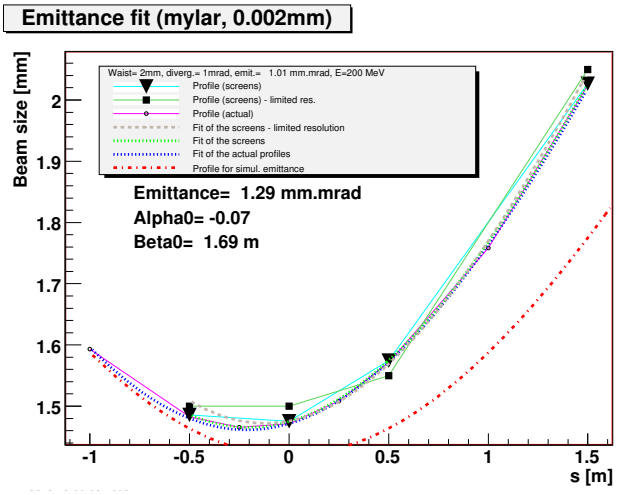

(b) 500 MeV

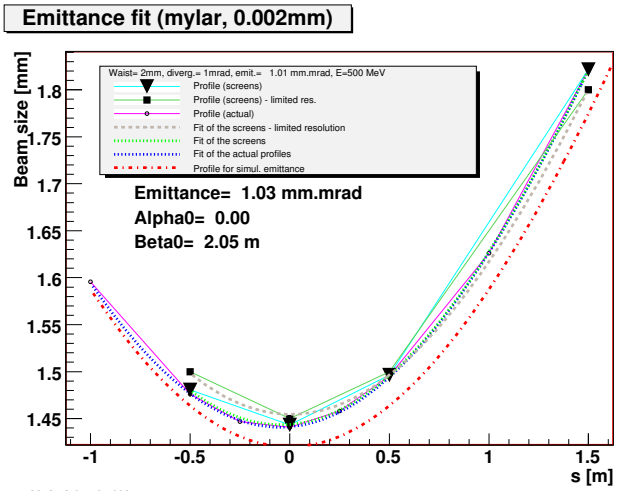

Figure 1.17: Emittance fit using $2\mu m$-thick Mylar screens at 200 MeV (a) and 500 MeV (b). The black squares show the beam size observed on each screen, the black triangles show the beam size rounded to the nearest 50 μm (to simulate what is observed by a camera with a limited pixel size). The open circles are the position measured at additional intermediate positions. The dashed brown line shows the emittance fit made using the black triangles. The dashed green line shows the emittance fit made using the black square. The dashed green line shows the emittance fit made using the open circles. The dashed red line is the theoretical profile of the beam assuming $\alpha_0 = 0$, $\beta_0 = 2.0m$ and $\epsilon = 1.01mm.mrad$. The values given on the plot below the legend for the emittance, α_0 and β_0 are those extracted from the fit on the beam sizes with limited pixel size.

1.4.5 Feasibility of transverse emittance measurement based on multiple OTRs

Based on our study we concluded that introducing simultaneously 4 screens in a beam line could be used to fit the Twiss parameters of an electron beam in a single shot measurement. We have shown that by using $2\mu m$-thick Mylar screen such fit would lead to a measurement of the beam transverse emittance correct within 15% for a 500 MeV beam and within 30% for a 200 MeV beam.

1.4.6 Experimental tests

Following this note we attempted to demonstrate such measurements at the same time than the extended pepper-pot described in section 1.3. The first tests were done at the Beam Test Facility at SPARC (see image 1.18) using the beam line shown on figure 1.19. Although this validated the principle the experiment had some data acquisition issue due to computers synchronism and we decided to repeat it at the Diamond Light Source and the results of that experiment have been published in [19].

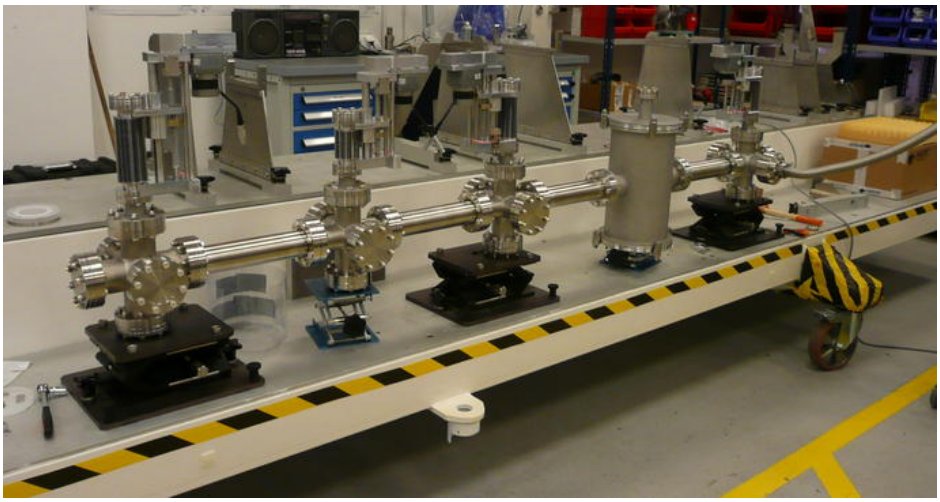

Figure 1.18: The multiple OTR and pepper-pot test beam line during a test installation at the Diamond Light Source before its shipment to Frascati.

The most important check to validate our method was to demonstrate that the beam size on the final screen was not affected by the insertion of other screens. This was done by measuring the beam size on the fourth screen (OTR4) with different configurations of the other three screens as shown on figure 1.20. As can be seen on that image no change in beam size was seen in x and a 5% change was seen in y. Using the beam size measured on each of the four screen it was then possible to measure the emittance. The beamline where the screens were installed had a non zero dispersion and this effect had

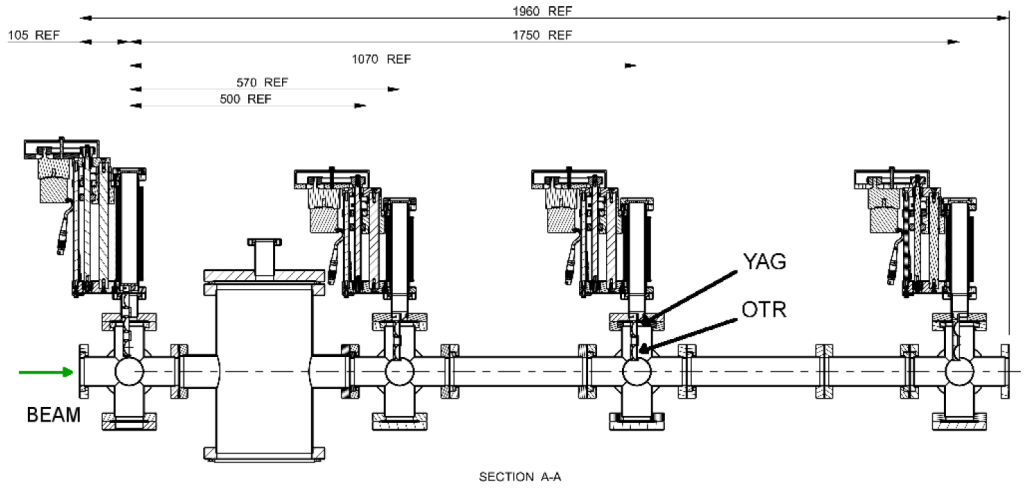

Figure 1.19: XXX The multiple OTR and pepper-pot test beam line during a test installation at the Diamond Light Source before its shipment to Frascati. Image taken from [19].

to be taken into account as described in [19]. Using this method we found a transverse emittance $\epsilon_x = 160.1\,\text{nm mrad} \pm 11.5\,\text{nm mrad}$ in very good agreement with the emittance measured by a quadrupole scan performed immediately after and that gave an emittance of $\epsilon_x = 162\,\text{nm mrad}$.

Criticism: OTR interferences

When we first proposed this experiment some colleagues warned us that according to [24] we would face difficulties due to interferences between the screens as they were located in the pre-wave zone of each other.

The so-called pre-wave zone is the area located with a distance $L_{\text{pre-wave}} = \lambda\gamma^2$ of a source of radiation produced by electrons. In our case $L_{\text{pre-wave}} \simeq 18\,\text{m}$. In the pre-wave the forward radiation from one screen can interfere with the backward radiation from the downstream screen and this should produced an interference effect. It should be noted that this interference effect is very sensitive to the observed wavelength.

As can be seen on figure 1.21 we did not see this effect. Further worked on these interferences has been presented in 2015 and confirmed that our setup was not subject to such interferences [25] as our images were integrated over a large number of wavelengths.

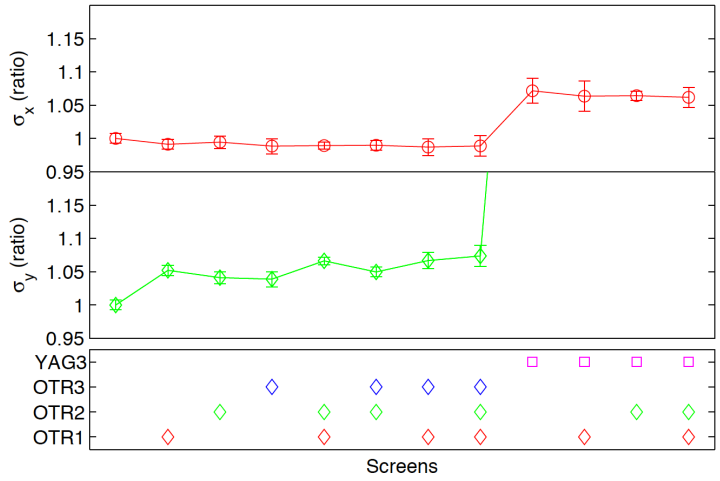

Figure 1.20: Beam size on the fourth OTR screen during the Diamond Tests as function of the screens inserted upstream. We can see that the effect of the upstream screens on the beam size measured on the lat screen is negligible in x and about 5% in y as was expected from our calculations. Image taken from [19].

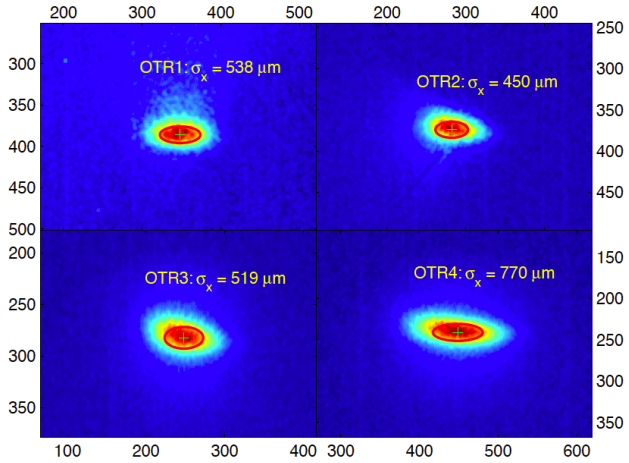

Figure 1.21: Beam size on the fourth OTR screen during the Diamond Tests as function of the screens inserted upstream. We can see that the effect of the upstream screens on the beam size measured on the lat screen is negligible in x and about 5% in y as was expected from our calculations. Image taken from [19].

1.5 Other techniques: Emulsion based measurement and masked OTR

The initial work on single shot emittance measurement included two other techniques. These techniques were more challenging and have been fully developed following the success of the techniques described above.

1.5.1 Emulsion based emittance measurement

Nuclear emulsions have a resolution of the order a few micrometers per hit that is a factor 10 better than CCD pixels (an example of such image is shown on figure 1.22). Given the low charge and high divergence of the beams produced by laser-driven plasma accelerator the beam reach such density after one or two meters and I investigated with several project students if this could be used to measure the transverse emittance of such beam as shown on figure 1.23.

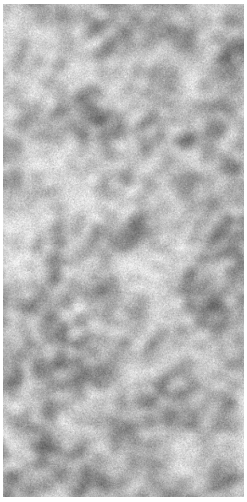

Figure 1.22: Image of electrons on nuclear emulsions. Image taken form [26].

At first it was difficult to recover the knowledge of the use of emulsions but we soon were able to observe in a microscope the tracks left by a radioactive source on nuclear emulsions and measure the position of individual hit [26]. Another student [27] showed that by using a technique called "image registration" we would be able to match several plates of emulsions located one after the other and reconstruct correctly the emittance (see figure 1.24) [28]. The conclusion of this work was that the emulsion technique would be best suited for low density beams.

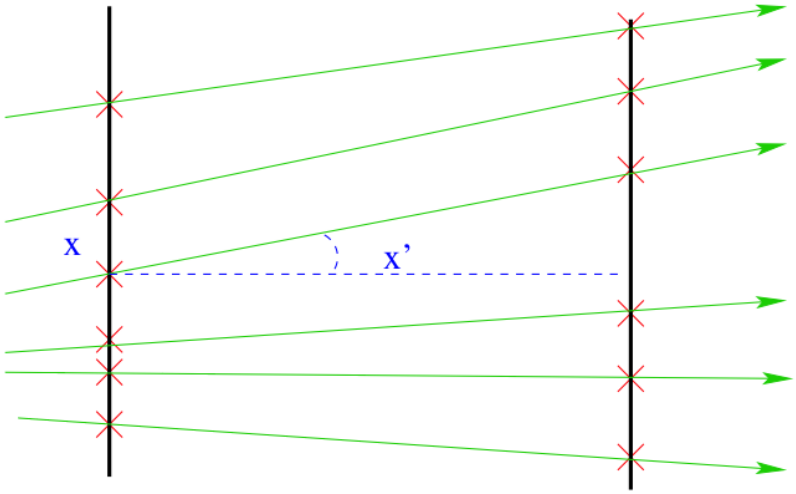

Figure 1.23: Emittance measurement using nuclear emulsions tracking.

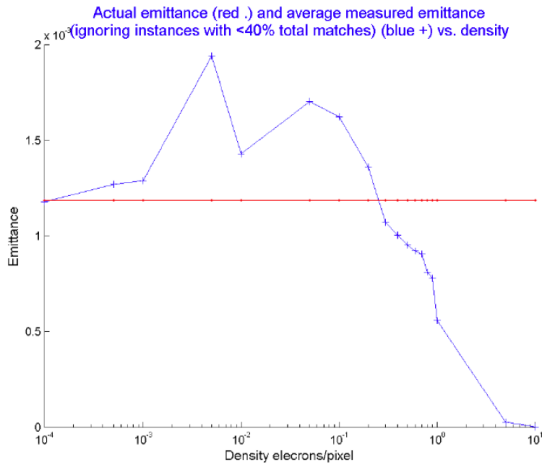

Figure 1.24: Accuracy of the emittance reconstruction depending on the electrons density (simulations taken from [28]).

1.5.2 Masked OTR

Another technique that was investigated is the use of a mask positioned between an optical transition radiation screen and the imaging CCD as shown on figure 1.25.

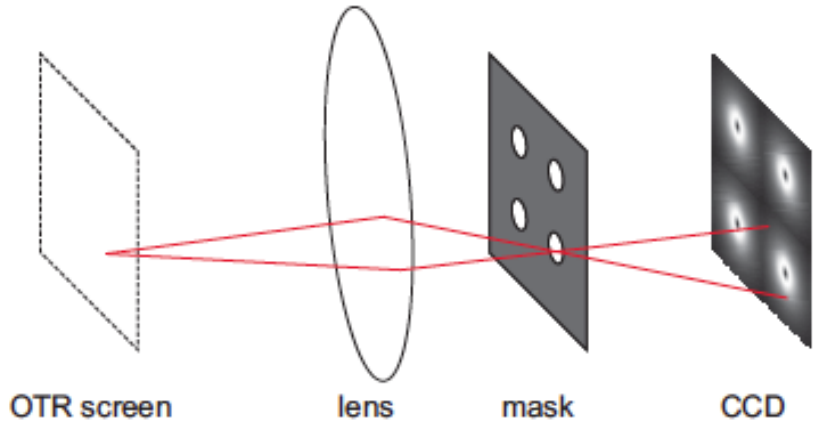

Figure 1.25: Layout of the masked OTR setup as taken from [29].

The principle of this measurement is that when they are produced the OTR photons take the direction of the incoming electrons. The spread in direction of emission of these photons is therefore dependent on the transverse emittance of the beam. However the energy of the beam will add another smearing factor as the photons are emitted in a $1/\gamma$ cone. The addition of an out of focus masking element should allows to reconstruct this spread in direction of the photons and therefore to measure the quadratic sum of the beam transverse emittance with its energy.

Simulations were done to qualify the processus and they showed very encouraging results as far as energy reconstruction was concerned (see 1.26). However we did not have time to take it further to attempt to measure the energy spectrum or the transverse emittance. We also did not have the opportunity to test these results on a real beam as I stopped that work when I arrived in Orsay.

I am aware that at least another group has demonstrated the use of OTR to measure the energy of the beam[**?**]. I am not aware of any group having used OTR to measure a beam energy spectrum or transverse emittance.

1.6 Overview of emittance measurement

My work on transverse emittance measurement has led to the conception and on beam demonstration of several single shot transverse emittance measurement diagnostics. The

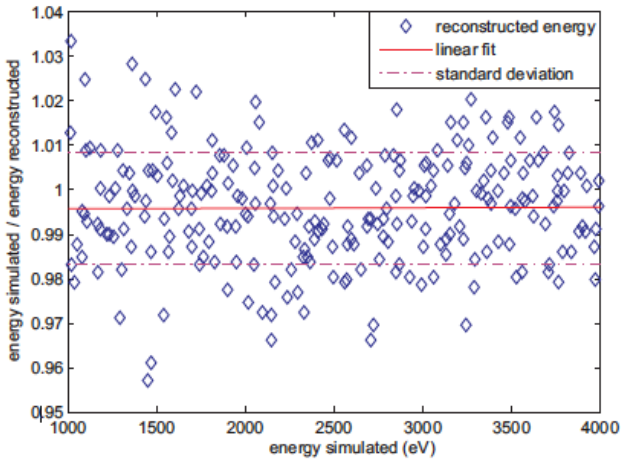

Figure 1.26: Simulations of energy measurements using masked OTR taken from [29].

figure 1.27 shows the type of beam parameters where each of these techniques apply.

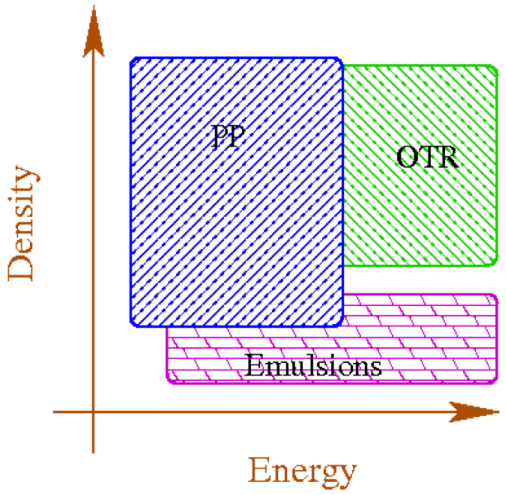

Figure 1.27: XXX Accuracy of the emittance reconstruction depending on the electrons density (simulations taken from [28]).

1.7 Undefined references

chap:plasmaAccelerationMecanism chap:laser-wire chap:pepper-pot chap:SP laser-synch

Bibliography

[1] J. Faure et al. A laser-plasma accelerator producing monoenergetic electron beams. *Nature*, 431:541–544, 2004.

[2] C. G. R. Geddes et al. High-quality electron beams from a laser wakefield accelerator using plasma-channel guiding. *Nature*, 431:538–541, 2004.

[3] S. P. D. Mangles et al. Monoenergetic beams of relativistic electrons from intense laser-plasma interactions. *Nature*, 431:535–538, 2004.

[4] W. P. Leemans S. M. Hooker et al. Gev electron beams from a centimetre-scale accelerator. *Nature Physics*, 2:696–699, 2006.

[5] Ian Blumenfeld, Christopher E. Clayton, Franz-Josef Decker, Mark J. Hogan, Chengkun Huang, Rasmus Ischebeck, Richard Iverson, Chandrashekhar Joshi, Thomas Katsouleas, Neil Kirby, Wei Lu, Kenneth A. Marsh, Warren B. Mori, Patric Muggli, Erdem Oz, Robert H. Siemann, Dieter Walz, and Miaomiao Zhou. Energy doubling of 42[thinsp]gev electrons in a metre-scale plasma wakefield accelerator. *Nature*, 445(7129):741–744, 02 2007.

[6] M. Zhang. Emittance formula for slits and pepper-pot measurement. *Fermilab-TM-1988, October*, 1996.

[7] Nicolas Delerue. Single Shot Transverse Emittance Measurement of multi-MeV Electron Beams Using a Long Pepper-Pot. *Nucl. Instrum. Meth.*, A644:1–10, 2011.

[8] M. McCann. Measuring low energy beam emittance using the pepper pot method. *Summer internship report*, 2007.

[9] S. Agostinelli et al. Geant4: A simulation toolkit. *Nucl. Instrum. Meth.*, A506:250–303, 2003.

[10] J. Hewlett. Pepperpot report. *Summer internship report*, 2007.

[11] A. Ghigo, G. Mazzitelli, F. Sannibale, P. Valente, and G. Vignola. Commissioning of the DAFNE beam test facility. *Nucl. Instrum. Meth.*, A515:524–542, 2003.

[12] B. Buonomo, G. Mazzitelli, and P. Valente. Performance and upgrade of the DAFNE Beam Test Facility (BTF). *IEEE Trans. Nucl. Sci.*, 52:824–829, 2005.

[13] P. Valente, B. Buonomo, and G. Mazzitelli. Diagnostics and upgrade of the DAFNE Beam Test Facility (BTF). *Nucl. Phys. Proc. Suppl.*, 150:362–365, 2006. [,362(2006)].

[14] Nicolas Delerue et al. Single-Shot Emittance Measurement of a 508MeV Electron Beam Using the Pepper-Pot Method. In *Particle accelerator. Proceedings, 23rd Conference, PAC'09, Vancouver, Canada, May 4-8, 2009*, page TH5RFP065, 2010.

[15] C. Thomas, N. Delerue, and R. Bartolini. Single shot 3 GeV electron transverse emittance with a pepper-pot. *Nuclear Instruments and Methods in Physics Research Section A: Accelerators, Spectrometers, Detectors and Associated Equipment*, 729:554–556, 2013.

[16] W. M. Yao et al. Review of particle physics. *J. Phys.*, G33:1–1232, 2006.

[17] Electron beam transverse emittance measurement optical transition radiation interferometry. 1996.

[18] Methods of emittance measurement. 1988.

[19] C Thomas, N Delerue, and R Bartolini. Single shot transverse emittance measurement from otr screens in a drift transport section. *Journal of Instrumentation*, 6(07):P07004, 2011.

[20] J. Rossbach and P. Schüser. Basic course on accelerator optics. *CERN Accelerator School*, CERN 94-01, 1994.

[21] Gerald R. Lynch and Orin I. Dahl. Approximations to multiple Coulomb scattering. *Nucl. Instrum. Meth.*, B58:6–10, 1991.

[22] J. Apostolakis et al. Geant4 low energy electromagnetic models for electrons and photons. CERN-OPEN-99-034.

[23] S. Chauvie et al. Geant4 low energy electromagnetic physics. Prepared for CHEP'01: Computing in High-Energy Physics and Nuclear, Beijing, China, 3-7 Sep 2001.

[24] V.A Verzilov. Transition radiation in the pre-wave zone. *Physics Letters A*, 273(1–2):135 – 140, 2000.

[25] M. Bergamaschi et al. Experimental study of optical transition radiation interference. In *RREPS'15*, volume Oral presentation of *RREPA*, https://indico.cern.ch/event/378549/contributions/1803855/, 2015.

[26] A. Simic. Electron tracking in nuclear emulsions. *Summer internship report*, 2007.

[27] N. Shipman. Using phase correlation for image registration. *Summer internship report*, 2008.

[28] N. Shipman. Study of emulsions data taken at the btf. *Summer internship report*, 2009.

[29] B.-J. Zandt. Otr simulations and measurements. *Project internship report*, 2008.